Received: 10 January 2023 | Accepted: 16 May 2023

DOI: 10.1002/jor.25629

Journal of Orthopaedic Research®

RESEARCH ARTICLE

3D T_1 relaxation time measurements in an equine model of subtle post-traumatic osteoarthritis using MB-SWIFT

Swetha Pala[1] | Nina E. Hänninen[1,2] | Ali Mohammadi[1] | Mohammadhossein Ebrahimi[1,2] | Nikae C. R. te Moller[3] | Harold Brommer[3] | P. René van Weeren[3] | Janne T. A. Mäkelä[1] | Rami K. Korhonen[1] | Isaac O. Afara[1] | Juha Töyräs[1,4,5] | Santtu Mikkonen[1] | Mikko J. Nissi[1] | Olli Nykänen[1,2]

[1]Department of Technical Physics, University of Eastern Finland, Kuopio, Finland

[2]Research Unit of Medical Imaging, Physics and Technology, University of Oulu, Oulu, Finland

[3]Department of Clinical Sciences, Faculty of Veterinary Medicine, Utrecht University, Utrecht, The Netherlands

[4]Science Service Center, Kuopio University Hospital, Kuopio, Finland

[5]School of Information Technology and Electrical Engineering, The University of Queensland, Brisbane, Queensland, USA

Correspondence
Mikko J. Nissi, Department of Technical Physics, University of Eastern Finland, POB 1627, 70211 Kuopio, Finland.
Email: mikko.nissi@uef.fi

Funding information
Pohjois-Savon Rahasto, Grant/Award Number: #65211960; Academy of Finland, Grant/Award Numbers: #285909, #315820, #319440, #324529, #325022, #325146, #337550; Suomen Kulttuurirahasto, Grant/Award Number: #00180787; Nederlandse Organisatie voor Wetenschappelijk Onderzoek, Grant/Award Number: 022.005.018; Dutch Arthritis Association, Grant/Award Number: LLP- 22

Abstract

The aim of this study is to assess whether articular cartilage changes in an equine model of post-traumatic osteoarthritis (PTOA), induced by surgical creation of standard (blunt) grooves, and very subtle sharp grooves, could be detected with ex vivo T_1 relaxation time mapping utilizing three-dimensional (3D) readout sequence with zero echo time. Grooves were made on the articular surfaces of the middle carpal and radiocarpal joints of nine mature Shetland ponies and osteochondral samples were harvested at 39 weeks after being euthanized under respective ethical permissions. T_1 relaxation times of the samples ($n = 8 + 8$ for experimental and $n = 12$ for contralateral controls) were measured with a variable flip angle 3D multiband-sweep imaging with Fourier transform sequence. Equilibrium and instantaneous Young's moduli and proteoglycan (PG) content from OD of Safranin-O-stained histological sections were measured and utilized as reference parameters for the T_1 relaxation times. T_1 relaxation time was significantly ($p < 0.05$) increased in both groove areas, particularly in the blunt grooves, compared with control samples, with the largest changes observed in the superficial half of the cartilage. T_1 relaxation times correlated weakly ($R_s \approx 0.33$) with equilibrium modulus and PG content ($R_s \approx 0.21$). T_1 relaxation time in the superficial articular cartilage is sensitive to changes induced by the blunt grooves but not to the much subtler sharp grooves, at the 39-week timepoint post-injury. These findings support that T_1 relaxation time has potential in detection of mild PTOA, albeit the most subtle changes could not be detected.

KEYWORDS

equine model, post-traumatic osteoarthritis, proteoglycan content, quantitative MRI, T_1 relaxation

1 | INTRODUCTION

Post-traumatic osteoarthritis (PTOA) develops as a result of joint injuries, such as fractures, articular cartilage lesions, cruciate or collateral ligament rupture, acute meniscal tears, or a combination of these. The resulting degenerative changes in the articular cartilage persist long after the initial injury[1,2] and may trigger progressive cartilage loss.[3] In the early stages of the degeneration, macromolecules of the cartilage are affected: the proteoglycan (PG) content decreases, accompanied by an increase in water content. These changes are followed by disruption of the collagen network.[3,4] Consequently, changes in the biomechanical properties of articular cartilage are associated with the onset of osteoarthritis (OA).[5]

Early interventions, such as repairing the damaged tissue, or stabilizing the joint, can limit the progression of PTOA[6] and hence early detection of articular cartilage damage is a great asset in the prevention and treatment of joint disease.[7] However, current non-invasive imaging methods[8,9] either lack sensitivity to detect subtle, early damage in PTOA, or are not yet available for clinical use.

Quantitative magnetic resonance imaging (qMRI) techniques can evaluate the compositional and structural changes in cartilage. A common qMRI parameter, T_1 relaxation time, is dictated by the local field fluctuations at frequencies nearby the MRI resonance frequency of the water protons. The high concentration of macromolecules in healthy cartilage increases the probability of having frequencies of molecular motions near the resonant frequency, shortening the T_1 relaxation time. In degenerated cartilage, the increased hydration of the depleted extracellular matrix moves the frequencies of molecular motion to less effective relaxation, prolonging the T_1 relaxation time, which is thus concomitant with the reduction of the mechanical stiffness.[10–12] Native T_1 relaxation time has shown promise in the detection of articular cartilage damage in animal models of PTOA,[11,13,14] correlating well with both biomechanical properties[11,13,14] and water content,[10] and is one of the most sensitive univariate parameters for assessing cartilage degeneration.[11]

Sweep imaging with Fourier transform (SWIFT) is a technique capable of capturing signals from the most rapidly relaxing spins.[15,16] Studies have reported accurate T_1 quantification using variable flip angle (VFA)-SWIFT.[17–19] Multiband SWIFT (MB-SWIFT)[20] is based on multiband excitation, which allows reaching a very high bandwidth with relatively low radiofrequency (RF) power. Although both are inherently ultrashort echo time (TE) three-dimensional (3D) sequences, the use of multiple excitation bands and thus higher bandwidth in MB-SWIFT distinguishes it from regular SWIFT.[20] MB-SWIFT's ability to achieve a zero TE coupled with reduced sensitivity to susceptibility artifacts and motion further support the use of the technique for quantification of T_1 in both ex vivo and in vivo conditions. Taken together, VFA-based T_1 measurement utilizing MB-SWIFT readout has a lot of potential in the diagnostics of joint-diseases such as PTOA. However, the sensitivity of this methodology for detection of subtle changes in articular cartilage caused by mild PTOA is not known and requires testing.

The articular groove model is an animal model for PTOA that was initially used in dogs,[21–23] and later expanded to sheep and rats.[24,25] Later, it has also been applied to the metacarpophalangeal joint of the horse.[26] The close similarity between the human and equine articular cartilage makes it an interesting model to study PTOA changes in cartilage.[27] Recently, the groove model was used in a 9-month study in the horse, comparing classic bluntly made grooves with sharp grooves that provoked hardly any tissue loss.[28] Material from this study was deemed optimal for testing our hypothesis that T_1 relaxation time measured with VFA-MB-SWIFT is sensitive to structural and/or compositional changes caused by mild PTOA. We therefore studied the bluntly and sharply grooved samples together with controls from the horse study[28] and correlated the outcome with biomechanical and histological properties of the tissue.

2 | METHODS

2.1 | Sample preparation

In a comprehensive study exploring the groove model for equine PTOA, nine healthy adult female Shetland ponies (aged between 4 and 13 years) underwent a surgical procedure in which each pony had one radiocarpal and one middle carpal joint bluntly or sharply grooved in one randomly assigned front limb per animal.[28] Three grooves in total (two in parallel in palmaro-dorsal and one in mediolateral directions) were created on the articular surfaces (Figure 1A,B) of the radial facet of the third carpal bone (middle carpal joint) and the intermediate carpal bone (radiocarpal joint) of equine subjects (Figure 1). The surgical procedure was performed under approval of the Utrecht University Animal Experiments Committee and the Central Committee for Animal Experiments (permit AVD108002015307) and in compliance with the Dutch Act on Animal Experimentation. The ponies were subjected to an 8-week incremental exercise program on a treadmill starting 3 weeks after surgery. After this, they were given free pasture exercise until euthanasia at 39 weeks after surgery. A more comprehensive description of experimental design and procedures is given elsewhere.[28]

A subset of samples used in a previous study[29] (8 bluntly and 8 sharply grooved osteochondral samples along with 12 samples from contralateral control limbs) were imaged in this study.

2.2 | MRI

MRI experiments were carried out on two different 9.4 Tesla preclinical Varian/Agilent scanners (Vnmrj DirectDrive console v. 3.10) using the same 19 mm quadrature RF volume transceiver (Rapid Biomedical GmbH) on both. The samples were mounted on custom-made sample holders and immersed in a test tube filled with phosphate-buffered saline (PBS) containing enzyme inhibitors, with the normal of the articular surface broadly perpendicular to the main

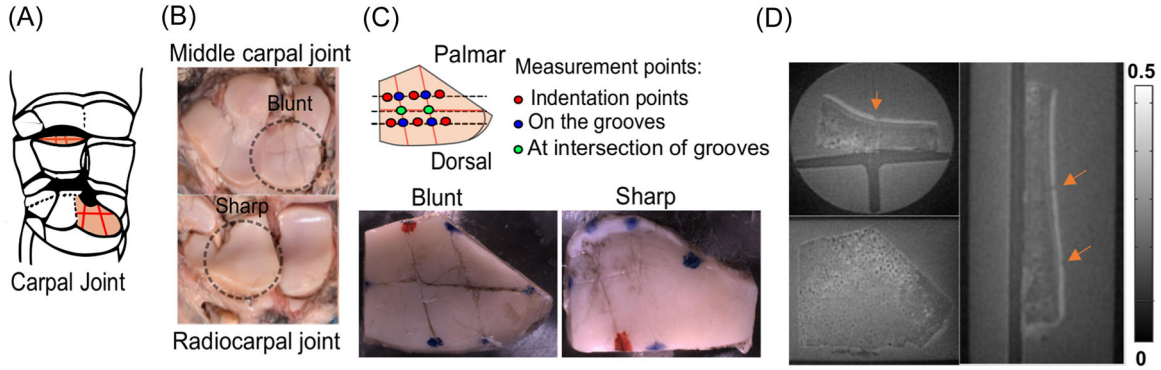

FIGURE 1 Schematic drawing of the right equine carpal joint (A), showing the grooved sites on the intermediate carpal bone in the radiocarpal joint and on the radial facet of the third carpal bone in the middle carpal bone with pictures of the corresponding surfaces where the grooved areas are indicated with dashed circles (B), drawing of a grooved joint surface showing the groove pattern (red lines) with biomechanical testing locations (red dots), and all 12 measurement points (six adjacent to grooves [red dots] and six on grooves [blue and green dots]) and pictures of typical examples of osteochondral samples with grooved surfaces (C), orthogonal slices through a three-dimensional (3D) volume averaged from 3D images acquired at flip angles 5°, 6°, 7°, 8°, 10°, and 14°. The arrows point at groove locations (D).

field (B_0), at the center of the RF coil. T_1 mapping was carried out by means of VFA measurement using 11 flip angles spanning 1°–20° (1°–8°, 10°, 14°, and 20°). A 3D radial MB-SWIFT sequence with bandwidth of 385 kHz, TR of 2.97 ms, 16,384 spokes per flip angle, field-of-view (3 cm), matrix size of 256,[3] and 32 dummy projections before spatial encoding was utilized as the read-out sequence. VFA was selected as the T_1 relaxation time measurement method over another common technique termed Look–Locker,[30] as it has a higher signal-to-noise ratio.[31] As the imaging was conducted using small tissue samples, impactful B_1+ variations (that could pose problems for the VFA technique) were not expected with the samples.

2.3 | Reference methods

Before the MRI, the osteochondral samples underwent biomechanical indentation testing, as reported previously.[29] For each sample, six measurement locations (three points each on the dorsal and palmar parts of the cartilage surface) were chosen.

The calculated Young's moduli from equilibrium and instantaneous (peak force after displacement) stress/strain ratios were corrected using Hayes equation[32] and Poisson ratios of $v = 0.2$[33] and $v = 0.5$,[34,35] respectively.

After the MRI, PG content was measured as OD, obtained from digital densitometry (DD) images of Safranin-O–Fast-Green-stained histological sections,[29] matching the locations subjected to biomechanical testing and MRI. Similar to the procedure reported by Mohammadi et al.,[29] OD analysis in this study was conducted for 12 regions of interest (ROIs) per sample, to estimate the depth-wise profiles through cartilage thickness, with a width of 1 mm using custom-made code in Matlab software (R2019, Mathworks). These 12 ROIs included the 6 biomechanical indentation testing locations, 4 locations at the grooves running in palmaro-dorsal direction and 2 at the intersection of grooves (Figure 1C). The depth-wise profiles were obtained for the superficial half and for the full cartilage thickness.

2.4 | MRI data processing

VFA–MB-SWIFT images (Figure 1D) were reconstructed using an iterative gridding algorithm.[36] For imaging experiments, T_1 relaxation time maps were fitted using nonlinear Gauss-Newton minimization in a voxel-wise manner (Equation 1).

$$S_0, T_1 = \operatorname{argmin} S_0, T_1 \left\| \sum_{j=1}^{N} S(\alpha_j) - S_0 \cdot \frac{\sin(\alpha_j) 1 - e^{-\mathrm{TR}/T_1}}{1 - \cos(\alpha_j) e^{-\mathrm{TR}/T_1}} \right\|^2 \quad (1)$$

where S_0 is the initial signal, α_j is the individual flip angle, and N is the number of flip angles.

2.5 | MRI data analysis

Depth-wise mean profiles of the T_1 relaxation time values from the grooves, regions adjacent to the grooves and at their intersections were calculated in cylindrical 3D volumes-of-interest (VOIs) (width ≈ 4 voxels and height ≈ 20 voxels (depending on cartilage thickness), covering the whole cartilage layer and some parts of background and bone). Similar profiles were also obtained from the control samples. A total of $n = 12$ VOIs were defined per sample, of which $n = 6$ VOIs were placed in the adjacent regions (carefully matched with the biomechanical testing points) and $n = 6$ VOIs were placed directly on the grooved regions (four on groove lines between the mechanical testing points and two on the intersections of the groove lines) (Figure 1C). A similar spatial pattern of VOI placement was used for the contralateral control samples. Before the analysis, the depth-wise T_1 profiles from the cylindrical VOIs were trimmed to obtain just the

cartilage profile while leaving out the bone and PBS and then interpolated to 10 depth-wise points. For further quantitative analysis, the mean T_1 relaxation times were computed from these trimmed profiles. VOI calculations and analyses were performed using an in-house written tool in Matlab.

Parametric surface maps were created to visualize the differences between the grooved regions and their adjacent regions. As a part of this, a triangulated 3D mesh was generated for the articular cartilage using a threshold-based multislice segmentation technique on the 6° flip angle magnitude images. Surface normals for each triangle were then calculated for the mesh. After this, the 3D T_1 relaxation time maps were sampled from within the cartilage volume along the surface normals. The sampled volume was then eroded from the surface side to remove partial volume effects from the surrounding PBS. Finally, mean T_1 values calculated along the surface normals were displayed as a surface map on the mesh. The 3D triangular meshes for cartilage surface were computed using Materialize Mimics (Materialise NV).

2.6 | Statistical analysis

The statistical analyses were carried out using a linear mixed-effects (LME) model, with T_1, OD (both from full-depth and half-depth regions), and equilibrium and instantaneous Young's moduli as the dependent variables. Samples from adjacent, grooved, and their intersection regions were considered all together for controls in statistical analysis, and samples from grooves and their intersection regions were together considered as grooves in LME analysis (to limit the number of possible comparisons). The ponies were selected as subject for random effects, accounting for additional covariance caused by taking observations from multiple locations within the same animal. The types of cartilage surface (control tissue, tissue at the grooves and tissue adjacent to the grooves for both groove types) were set as fixed variables, and the scanner information was considered as a covariate in the analysis of T_1. As only a subset of the specimens from the previous studies[28,29] were used in this study, all the data-analyses were redone. In addition, partial correlation analysis was performed to evaluate the relationships between the OD, T_1 relaxation times and the equilibrium and instantaneous Young's moduli. A $p < 0.05$ was considered as the limit of statistical significance. The normality test (Shapiro–Wilk) was used to check for normal distribution of T_1 and reference data, and, depending on this either Pearsons' (R_p) or Spearmans' (R_s) partial correlations were used, and approximate linearity of the dependent variables was achieved. All statistical analyses were carried out using IBM SPSS statistics (v. 27 SPSS, IBM Company).

3 | RESULTS

3.1 | Qualitative analysis of MRI data

Surface maps of the relaxation times in cartilage showed visual differences between the lesioned cartilage and adjacent tissue in the bluntly grooved samples. The damage was, however, not visually detectable in the samples with sharp grooves (Figure 2).

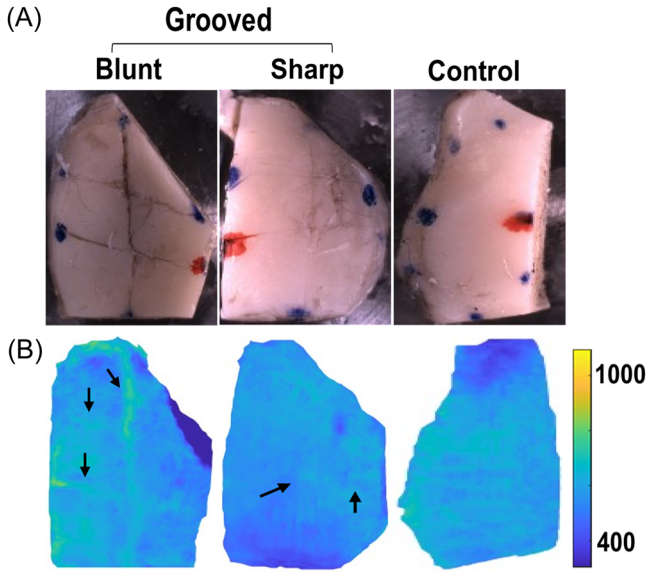

FIGURE 2 Photographs of the specimens (A) and the corresponding surface T_1 relaxation time maps (B). Cartilage surface maps calculated with a segmented mesh could differentiate between the defective regions from bluntly grooved regions and their adjacent regions, highlighted with black arrows. Sharp grooves were visually almost indistinguishable from the adjacent regions.

T_1 relaxation time maps revealed an increase in T_1 values between the grooved groups with respect to controls, especially at the grooved regions of bluntly grooved samples (Figure 3A). Changes at groove regions in T_1 followed the trend of changes in OD maps reflecting PG content, showing decreased PG content at the grooved regions especially with the blunt groove type (Figure 3B).

Visually evaluated profiles showed elevated T_1 values at the grooves and at groove intersections with respect to controls (Figure 4A). Compared with controls, T_1 values of grooved samples appeared higher towards the superficial half of the cartilage at the grooves and their intersections. The T_1 relaxation times from both groove types overlap with those of the controls towards the deeper zones in depth-wise profiles. Samples with blunt groove injury showed higher T_1 values than sharply grooved samples in the depth-wise profiles at the grooves and intersections of those, for the superficial half of the cartilage (Figure 4A). However, the OD profiles showed a decrease of PG content for each anatomical location (adjacent to grooves, at grooves and groove intersections) with respect to controls (Figure 4B and Table 1).

3.2 | LME model analysis

Higher T_1 values were noted in bluntly and sharply grooved regions than in the respective adjacent areas in the following interaction groups: between the blunt grooves versus the adjacent regions, sharply grooved

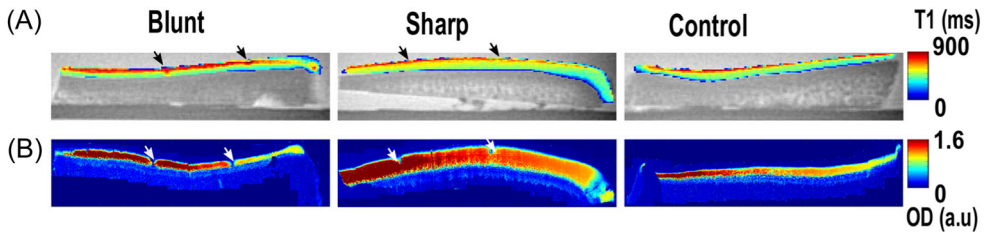

FIGURE 3 Coronal axis T_1 relaxation time maps (A) of seven consecutive slices averaged through the groove points and the corresponding optical densitometry measurement maps (B) from blunt and sharp grooved articular cartilage (groove locations marked with black and white arrows) and a contralateral control joint (with intact articular cartilage surface). Between the groove types, blunt grooves are well detectable in comparison with sharp grooves on the articular surface of the carpal joint.

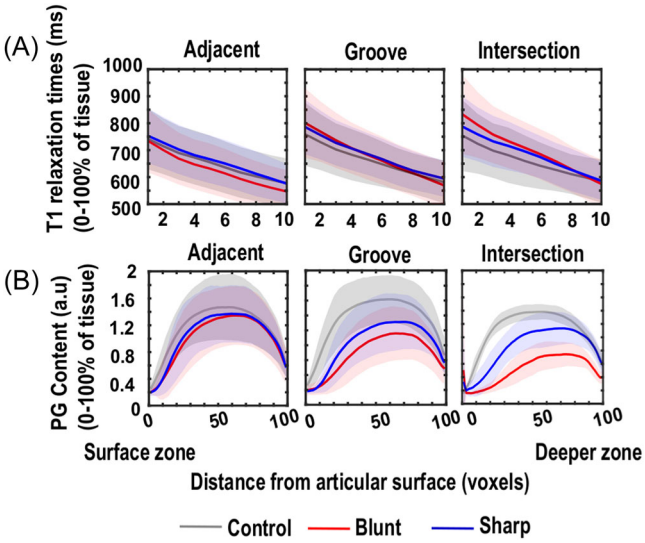

FIGURE 4 T_1 relaxation times (A) and OD profiles (B) sampled and depth-normalized from the adjacent locations that also served as biomechanics testing locations, groove locations, and groove intersections. T_1 profiles from groove and their intersection locations indicate increased T_1 values in both groove types in the superficial half-depth with respect to controls, but comparatively higher in blunt grooves in the superficial part of the cartilage. OD profiles showed larger variations in the superficial half of the cartilage layer.

versus adjacent regions of bluntly grooved groups, adjacent regions of sharp grooves versus blunt grooves, and between adjacent regions of both bluntly and sharply grooved groups (Table 2). With respect to controls, significant differences with increased T_1 values were noted with both groove types: with the adjacent regions of bluntly grooved groups, with blunt grooves, and sharp grooves. In the superficial half of the tissue, there were larger and more significant differences in T_1 relaxation times than in full-depth cartilage, that is, between the bluntly grooved group and the adjacent regions of the sharply grooved group. With respect to controls, different significance levels were noted with adjacent regions to bluntly grooved group and with sharply grooved. In addition, significant differences were noted between sharp grooves and their adjacent regions (Figure 5A and Table 2).

The differences in T_1 relaxation times were mostly in line with PG content as measured by OD. However, with OD, the differences were noted in all regions of the grooved (blunt and sharp) groups compared with the corresponding regions in the controls, in both full-depth and superficial half-depth tissue. In addition to the differences noted between groups with full-depth T_1, OD showed also significant differences between control versus adjacent regions of sharp grooves, sharp grooves versus their adjacent regions, and blunt grooves versus sharp grooves. Compared with superficial half-depth T_1, there were additional significant differences between controls versus adjacent region of sharp grooves and sharp grooves versus blunt grooves (Figure 5B and Table 2). Biomechanical properties differ only between control and adjacent regions of sharp grooves (Table 2).

3.3 | Correlation analysis

For pooled data (grooved and control groups together), a weak but significant negative correlation between full-depth T_1 relaxation time and the equilibrium modulus ($R_p = -0.284$, $p = 0.000$) and instantaneous modulus ($R_s = -0.202$, $p = 0.012$) was found. In the superficial half of articular cartilage (0%–50%), slightly stronger correlations with equilibrium modulus ($R_s = -0.337$, $p = 0.000$) and with the instantaneous modulus ($R_s = -0.236$, $p = 0.003$) were observed. OD correlated weakly with T_1 in full-thickness cartilage ($R_s = -0.142$, $p = 0.014$) and in the superficial half of the cartilage ($R_s = -0.218$, $p = 0.000$) (Table 3).

4 | DISCUSSION

In this study, we investigated the potential of T_1 relaxation time, measured with VFA-MB-SWIFT, for the assessment of PTOA induced by surgically created grooves on the articular surfaces of the carpal joints in ponies. T_1 relaxation times were analyzed for changes, along with the reference properties of the articular cartilage measured via mechanical indentation testing (equilibrium modulus and instantaneous modulus) and DD (PG content). The findings indicated that the T_1 relaxation time of cartilage was altered due to the changes caused by the injuries and was dependent on the severity of the induced damage. Particularly, T_1 was sensitive to the

TABLE 1 Mean and 95% confidence intervals of each group for T_1 relaxation time, OD, and mechanical properties.

Groups	Mean	95% Confidence intervals Lower bound	Upper bound	Mean	95% Confidence intervals Lower bound	Upper bound
	Superficial-half T_1 relaxation times (ms)			Full-depth T_1 relaxation times (ms)		
C	703.586	686.198	720.974	657.382	642.587	672.178
SA	706.475	684.736	728.213	659.667	640.773	678.560
SG	734.687	712.948	756.426	681.392	662.498	700.285
BA	678.729	656.991	700.468	629.014	610.121	647.907
BG	750.679	728.941	772.418	686.026	667.133	704.919
	Superficial-half OD (a.u.)			Full-depth OD (a.u.)		
C	0.846	0.722	0.970	0.991	0.882	1.099
SA	0.494	0.371	0.617	0.634	0.527	0.742
SG	1.097	0.981	1.212	1.163	1.068	1.258
BA	0.918	0.787	1.048	1.048	0.930	1.165
BG	0.696	0.570	0.822	0.863	0.751	0.975
	Equilibrium modulus (MPa)			Instantaneous modulus (MPa)		
C	1.114	1.006	1.222	7.562	6.326	8.798
SA	0.928	0.810	1.046	6.275	5.014	7.536
BA	1.021	0.904	1.139	6.706	5.451	7.962

Notes: Groups in the table are noted. Intersections are included in groove regions.

Abbreviations: BA, adjacent regions of blunt grooves; BG, bluntly grooved regions; C, controls; SA, adjacent regions of sharp grooves; SG, sharply grooved regions.

TABLE 2 Mean differences and their significances.

Comparisons between groups	Full-depth T_1 (ms)	Superficial-half T_1 (ms)	Full-depth OD (a.u.)	Superficial-half OD (a.u.)	Equilibrium modulus (MPa)	Instantaneous modulus (MPa)
C vs. BA	28.368*	24.857**	0.172*	0.251*	–	–
C vs. SA	–	–	0.116**	0.179*	0.186*	1.287**
C vs. BG	28.644*	47.093*	0.529*	0.603*	NA	NA
C vs. SG	24.009**	31.101*	0.300*	0.401*	NA	NA
BA vs. SA	30.652**	27.745**	–	–	–	–
BG vs. SG	–	–	0.229*	0.202*	NA	NA
BA vs. BG	57.012*	71.952*	0.357*	0.352*	NA	NA
SA vs. SG	–	28.212**	0.185*	0.222*	NA	NA
BA vs. SG	52.372*	55.958*	0.128**	0.150**	NA	NA
SA vs. BG	26.360**	44.205**	0.413*	0.424*	NA	NA

Note: Mean differences and their significances obtained via linear mixed effect model-based comparisons between groups for T_1 relaxation times, NA, not applicable; OD, and mechanical properties. Groups in the table are noted. Intersections are included in groove regions.

Abbreviations: BA, adjacent regions of bluntly grooved; BG, bluntly grooved regions; C, controls; SA, adjacent regions of sharp grooves; SG, sharply grooved regions.

*Indicate differences with significances of $p < 0.01$.

**indicates significances of $p < 0.05$.

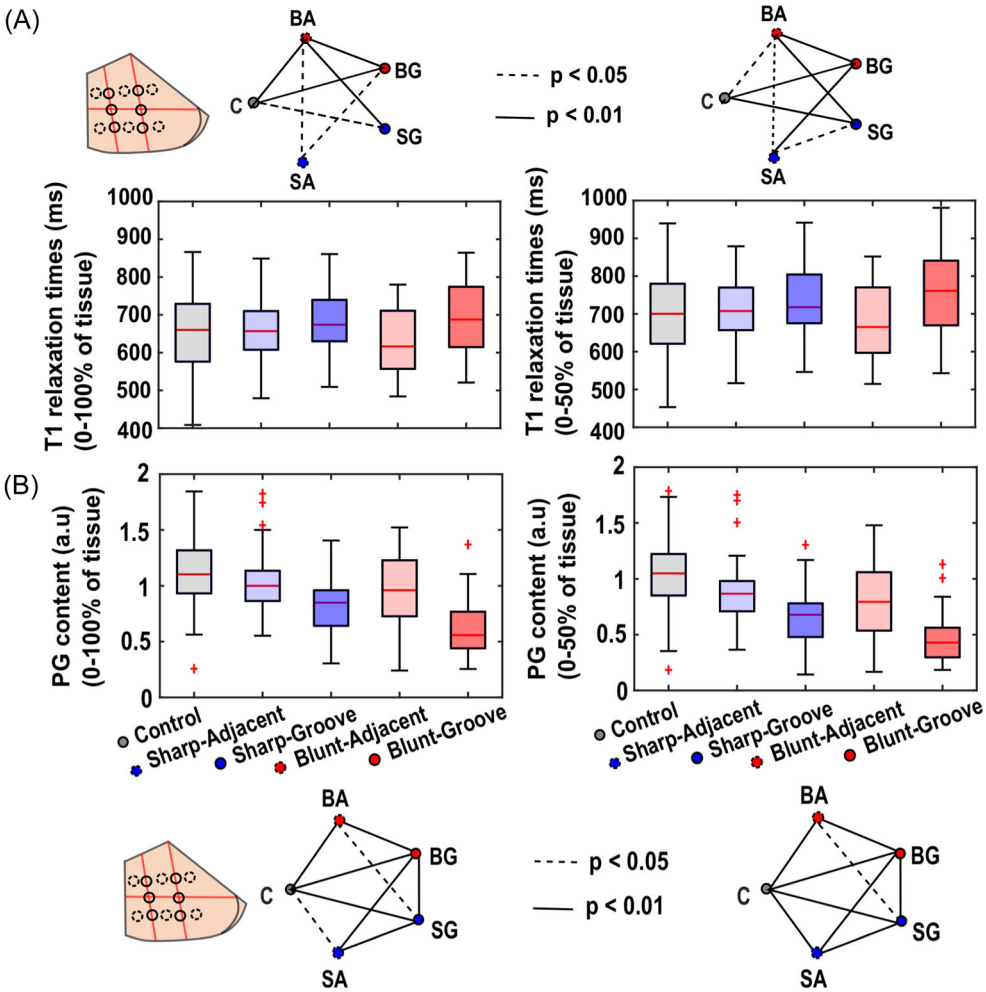

FIGURE 5 Boxplots of T_1 relaxation times (A) and OD (B) from full-depth and from superficial zone, from all 12 measurement locations (6 adjacent to grooves, 6 on the grooves + intersections). Red lines are the median values of the measurements and red crosses indicate the outliers within the data limits. Star diagrams above and below illustrate the significant differences identified between the compared groups. BA, blunt adjacent; BG, blunt groove; C, controls; SA, sharp adjacent; SG, sharp groove.

TABLE 3 Correlation coefficients obtained from the partial correlation analysis.

	Correlation with equilibrium modulus		Correlation with instantaneous modulus		Correlation with OD	
	Anatomical location and scanner information as covariate					
T_1 relaxation time	Full-depth	Half-depth	Full-depth	Half-depth	Full-depth	Half-depth
	$R_s = -0.284$*	$R_s = -0.337$*	$R_s = -0.202$*	$R_s = -0.236$*	$R_s = -0.142$*	$R_s = -0.218$*

Note: Correlation coefficients obtained from the partial correlation analysis between T_1 relaxation time and the reference properties of articular cartilage for the two depths analyzed.

*Statistically significant ($p < 0.05$).

more advanced post-traumatic degeneration caused by the blunt grooves in the articular cartilage. The very early post-traumatic degeneration in the adjacent tissue to the sharp grooves was hardly distinguishable from controls based on the T_1 relaxation times. Tissue damage was easier to detect in the superficial 50% of the cartilage compared with full-depth cartilage. The study revealed weak negative correlations between the T_1 relaxation times and cartilage PG content and mechanical properties. Blunt grooves were well detectable in comparison to the sharp grooves from the average T_1 relaxation time maps in slices through the groove points and in the surface map visualizations by their higher T_1 relaxation times.

Higher T_1 values are broadly indicative of higher hydration of the cartilage tissue[10] due to, for example, more significant degenerative changes in the respective locations. In the adjacent regions, the changes were not large enough to cause a detectable increase in the T_1 relaxation time. For full-cartilage thickness, slightly smaller differences were noticed

between the compared groups than in the superficial 50% of the tissue. This was not unexpected since the damage caused by the grooves was most prominent in the superficial half of the cartilage and it should be noted that the sharp grooves were limited to the upper 400 μm of the cartilage. With larger changes in the superficial half of the cartilage, the model represents well the situation that OA changes in articular cartilage commonly initiate from the superficial half of cartilage.[37–39] The correlation of T_1 relaxation times with the DD-measured PG content of cartilage and the detected differences in T_1 between the grooved regions and controls or adjacent-to-damaged regions indicate that PG loss of cartilage or cartilage degeneration in general had an influence on T_1 values. These correlations of T_1 with the reference methods were weaker than in previous studies on naturally degenerated human cartilage,[13] enzymatically treated articular cartilage,[11] and in an equine defect model,[14] which showed correlations between $R = 0.5$ and 0.8. In this study, the correlations of T_1 with the equilibrium moduli were higher than those with OD, which is consistent with previous studies.[11,13,14] This outcome potentially indicates that the T_1 relaxation time in this groove model was also influenced by other degenerative processes, not just by the increase in free water content caused by PG loss at groove regions, although with such weak correlations, strong conclusions cannot be made. The stronger correlations for the T_1 relaxation times in the superficial half of the cartilage than in the full-depth are in line with the superficial location of the affected region.

Previous studies on articular cartilage[18,19] have shown the feasibility of measurement of T_1 relaxation times for a broader range of spin populations with VFA-SWIFT, and demonstrated increased T_1 values in trypsin-treated cartilage samples. As the trypsin treatment induces PG loss in articular cartilage, the increase in T_1 relaxation at the grooved regions with reduced PG content in this study is in line with the previous results. Several previous studies have shown that native T_1 relaxation time is sensitive to changes in the PG content and to the mechanical properties of the tissue.[9–11,14,28,37,39,40] Results of the current study are consistent with the previous studies in the sense that T_1 increase coincided with decreased PG content. However, the correlation found between the PG content and T_1 relaxation time was not as strong as reported in most of the previous studies. This could be due to the different methods of measuring T_1 but is more likely due to the very modest degree of degeneration in the present sample pool (especially in the sharply grooved group), with insufficient data spread for reliable correlation analysis. In a previous report,[19] it was noted that VFA-SWIFT has lower apparent T_1 relaxation time values (T_1 ranging between ~800 and 1800 ms) compared with measuring T_1 relaxation by inversion or saturation recovery sequences (T_1 between ~600 and 2400 ms). This shift in T_1 values and compression of the range of expected T_1 values could be one of the reasons for the observed low contrasts in the cartilage between the grooved and adjacent regions.

As reported in the previous study on the same equine model[29] with a slightly larger sample set than in this study, DD revealed degenerative changes in grooved and the adjacent regions. However, the biomechanical indentation testing in the previous study, conducted at the regions adjacent to the grooved tissue, showed a larger decrease in the sharply grooved than in the bluntly grooved group with respect to controls. The differences in observations between this and the previous study likely result from the different number of samples used in the study.

The current study is not without limitations. First, samples were immersed in PBS during imaging and thus the differentiation between the cartilage and background was not straightforward and may have resulted in inclusion of PBS or exclusion of the most superficial part of cartilage in the analyzed data. However, for cartilage segmentation from the PBS, careful evaluation of the depth-wise profiles was undertaken. Second, the exact biomechanical indentation testing sites and sites used for histology were not coregistered with the sites used for T_1. However, careful and consistent visual evaluations were followed to identify the locations of the biomechanical indentation testing and histology, which were then used for T_1 relaxation time analysis. Third, the sham-operated contralateral joints were considered as control samples, but there was no separate control group from non-operated horses. The sham-operated contralateral joints cannot be considered entirely free from structural alterations of the cartilage.[28,29] In particular bilateral inflammatory responses might have been induced because of repeated arthroscopies and arthrocentesis.[41] Fourth, due to technical constraints the full set of the samples from previous study could not be included and was not balanced between the control ($n = 12$ samples) and the grooved groups (sharp = 8, blunt = 8), which might have reduced the statistical power due to the asymmetric comparison. However, the relatively small sample sizes in the grooved groups did not significantly impair this study, as the goal was to investigate the feasibility of T_1 relaxation time mapping in detecting chronic changes due to lesions in grooved groups with respect to controls. Fifth, two different MRI scanners were utilized in this study due to hardware issues, which imposed an additional variable to be considered in the statistical analysis. Lastly, no B_1+ correction was applied in the VFA-based computation of T_1 relaxation time. However, the B_1+ field of the volume coil used in the study was carefully calibrated and was highly uniform within the relatively small specimens. Thus, the effects of B_1+ deviations on the T_1 measurements are expected to be minor and consistent between the samples.

In conclusion, this study reports the potential of T_1 relaxation time mapping in tracing the progression of modest PTOA in articular cartilage in surgically grooved tissue and its adjacent regions. The model utilized two different types of grooves featuring considerable differences in local tissue damage and appeared very suitable for the purpose of the study. The changes induced by the surgical model varied from modest in the blunt grooves to minimal in the sharp grooves. The T_1 relaxation times evaluated in small VOIs were highly sensitive to damage in the superficial half of the cartilage, especially at grooved regions in the bluntly grooved samples compared with healthy cartilage. The findings of this study suggest that T_1 as measured by VFA–MB-SWIFT is sensitive to modest tissue changes caused by PTOA, but cannot distinguish the mildest forms of damage in the adjacent tissues, which are also undetectable via biomechanical testing.

AUTHOR CONTRIBUTIONS

Mikko J. Nissi, Rami K. Korhonen, and Juha Töyräs were responsible for design of the study. Swetha Pala, Nina E. Hänninen, Mikko J.

Nissi, and Olli Nykänen were involved in MRI measurements, Ali Mohammadi, Nikae C. R. te Moller, Harold Brommer, P. René van Weeren, and Janne T. A. Mäkelä were responsible for indentation testing. Mohammadhossein Ebrahimi and Isaac O. Afara were responsible for OD measurements. Nikae C. R. te Moller, Harold Brommer, P.René van Weeren, and Janne T. A. Mäkelä were involved in animal experiments. Swetha Pala was responsible for data analysis and manuscript drafting. Swetha Pala, Mikko J. Nissi, and Olli Nykänen were involved in interpretation of results and critically revised the manuscript up to final version. All authors were involved in revision for intellectual content and final approval.

ACKNOWLEDGEMENTS

This study was made possible by the Academy of Finland projects (#285909, #319440, #324529, #325146, #325022, #337550, #315820), Finnish Cultural Foundation (#00180787), North-Savonia Regional Fund (#65211960), NWO Graduate Programme Grant (022.005.018), and support from the Dutch Arthritis Association grant LLP-22. This work was carried out with the support of Kuopio Biomedical Imaging Unit, University of Eastern Finland, Kuopio, Finland (part of Biocenter Kuopio, Finnish Biomedical Imaging Node, and EuroBioImaging). Support from Mr. Henri Leskinen with scripts for profile computation is gratefully acknowledged.

CONFLICT OF INTEREST STATEMENT

The authors declare no conflict of interest.

DATA AVAILABILITY STATEMENT

All raw data and documentation, as well as key analysis codes used in this study, are available for download at Zenodo (https://doi.org/10.5281/zenodo.7408554).

ORCID

Swetha Pala http://orcid.org/0000-0002-2149-5386
Nina E. Hänninen https://orcid.org/0000-0003-0392-8552
Ali Mohammadi http://orcid.org/0000-0001-6254-0879
Mohammadhossein Ebrahimi https://orcid.org/0000-0002-5480-7550
Nikae C. R. te Moller http://orcid.org/0000-0001-8675-330X
Harold Brommer https://orcid.org/0000-0002-3622-8571
P. René van Weeren http://orcid.org/0000-0002-6654-1817
Janne T. A. Mäkelä http://orcid.org/0000-0002-6123-1262
Rami K. Korhonen https://orcid.org/0000-0002-3486-7855
Isaac O. Afara https://orcid.org/0000-0001-7114-0439
Juha Töyräs https://orcid.org/0000-0002-8035-1606
Santtu Mikkonen http://orcid.org/0000-0003-0595-0657
Mikko J. Nissi http://orcid.org/0000-0002-5678-0689
Olli Nykänen http://orcid.org/0000-0001-7329-3463

REFERENCES

1. Yang KGA, Saris DBF, Verbout AJ, Creemers LB, Dhert WJA. The effect of synovial fluid from injured knee joints on in vitro chondrogenesis. *Tissue Eng*. 2006;12(10):2957-2964. doi:10.1089/ten.2006.12.2957
2. Wei L, Fleming BC, Sun X, et al. Comparison of differential biomarkers of osteoarthritis with and without posttraumatic injury in the Hartley guinea pig model. *J Orthop Res*. 2010;28(7):900-906. doi:10.1002/jor.21093
3. Buckwalter JA. Articular cartilage: injuries and potential for healing. *J Orthop Sports Phys Ther*. 1998;28(4):192-202. doi:10.2519/jospt.1998.28.4.192
4. Goldring MB, Goldring SR. Articular cartilage and subchondral bone in the pathogenesis of osteoarthritis. *Ann NY Acad Sci*. 2010;1192:230-237. doi:10.1111/j.1749-6632.2009.05240.x
5. Buckwalter JA, Anderson DD, Brown TD, Tochigi Y, Martin JA. The roles of mechanical stresses in the pathogenesis of osteoarthritis: implications for treatment of joint injuries. *Cartilage*. 2013;4(4):286-294. doi:10.1177/1947603513495889
6. Anderson DD, Chubinskaya S, Guilak F, et al. Post-traumatic osteoarthritis: improved understanding and opportunities for early intervention. *J Orthop Res*. 2011;29(6):802-809. doi:10.1002/jor.21359
7. Bolcos PO, Mononen ME, Tanaka MS, et al. Identification of locations susceptible to osteoarthritis in patients with anterior cruciate ligament reconstruction: combining knee joint computational modelling with follow-up T1ρ and T2 imaging. *Clin Biomech*. 2020;79(December 2018):104844. doi:10.1016/j.clinbiomech.2019.08.004
8. Brinkhof S, te Moller N, Froeling M, et al. T2* mapping in an equine articular groove model: visualizing changes in collagen orientation. *J Orthop Res*. 2020;38(11):2383-2389. doi:10.1002/jor.24764
9. Honkanen MKM, Mohammadi A, te Moller NCR, et al. Dual-contrast micro-CT enables cartilage lesion detection and tissue condition evaluation ex vivo. *Equine Vet J*. 2022;55:315-324. doi:10.1111/evj.13573
10. Berberat JE, Nissi MJ, Jurvelin JS, Nieminen MT. Assessment of interstitial water content of articular cartilage with T1 relaxation. *Magn Reson Imaging*. 2009;27(5):727-732. doi:10.1016/j.mri.2008.09.005
11. Nissi MJ, Salo EN, Tiitu V, et al. Multi-parametric MRI characterization of enzymatically degraded articular cartilage. *J Orthop Res*. 2016;34(7):1111-1120. doi:10.1002/jor.23127
12. Wayne JS, Kraft KA, Shields KJ, Yin C, Owen JR, Disler DG. MR imaging of normal and matrix-depleted cartilage: correlation with biomechanical function and biochemical composition. *Radiology*. 2003;228(2):493-499. doi:10.1148/radiol.2282012012
13. Rautiainen J, Nissi MJ, Salo EN, et al. Multiparametric MRI assessment of human articular cartilage degeneration: correlation with quantitative histology and mechanical properties. *Magn Reson Med*. 2015;74(1):249-259. doi:10.1002/mrm.25401
14. Kajabi AW, Casula V, Sarin JK, et al. Evaluation of articular cartilage with quantitative MRI in an equine model of post-traumatic osteoarthritis. *J Orthop Res*. 2021;39(1):63-73. doi:10.1002/jor.24780
15. Idiyatullin D, Corum C, Park JY, Garwood M. Fast and quiet MRI using a swept radiofrequency. *J Magn Reson*. 2006;181(2):342-349. doi:10.1016/j.jmr.2006.05.014
16. Idiyatullin D, Corum C, Moeller S, Garwood M. Gapped pulses for frequency-swept MRI. *J Magn Reson*. 2008;193(2):267-273. doi:10.1016/j.jmr.2008.05.009
17. Christensen KA, Grant DM, Schulman EM, Walling C. Optimal determination of relaxation times of Fourier transform nuclear magnetic resonance. determination of spin-lattice relaxation times in chemically polarized species. *J Phys Chem*. 1974;78(19):1971-1977. doi:10.1021/j100612a022
18. Wang L, Corum CA, Idiyatullin D, Garwood M, Zhao Q. T1 estimation for aqueous iron oxide nanoparticle suspensions using a variable flip angle SWIFT sequence. *Magn Reson Med*. 2013;70(2):341-347. doi:10.1002/mrm.24831
19. Nissi MJ, Lehto LJ, Corum CA, et al. Measurement of T1 relaxation time of osteochondral specimens using VFA-SWIFT. *Magn Reson Med*. 2015;74(1):175-184. doi:10.1002/mrm.25398

20. Idiyatullin D, Corum CA, Garwood M. Multi-band-SWIFT. *J Magn Reson*. 2015;251(1):19-25. doi:10.1016/j.jmr.2014.11.014
21. Marijnissen ACA, Van Roermund PM, Verzijl N, Tekoppele JM, Bijlsma JWJ, Lafeber FPJG. Steady progression of osteoarthritic features in the canine groove model. *Osteoarthritis Cartilage*. 2002;10(4):282-289. doi:10.1053/joca.2001.0507
22. Sniekers YH, Intema F, Lafeber FP, et al. A role for subchondral bone changes in the process of osteoarthritis: a micro-CT study of two canine models. *BMC Musculoskelet Disord*. 2008;9:20. doi:10.1186/1471-2474-9-20
23. Intema F, Sniekers YH, Weinans H, et al. Similarities and discrepancies in subchondral bone structure in two differently induced canine models of osteoarthritis. *J Bone Miner Res*. 2010;25(7):1650-1657. doi:10.1002/jbmr.39
24. Mastbergen SC, Pollmeier M, Fischer L, Vianen ME, Lafeber FPJG. The groove model of osteoarthritis applied to the ovine fetlock joint. *Osteoarthritis Cartilage*. 2008;16(8):919-928. doi:10.1016/j.joca.2007.11.010
25. de Visser HM, Weinans H, Coeleveld K, van Rijen MHP, Lafeber FPJG, Mastbergen SC. Groove model of tibia-femoral osteoarthritis in the rat. *J Orthop Res*. 2017;35(3):496-505. doi:10.1002/jor.23299
26. Maninchedda U, Lepage OM, Gangl M, et al. Development of an equine groove model to induce metacarpophalangeal osteoarthritis: a pilot study on 6 horses. *PLoS One*. 2015;10(2):e0115089. doi:10.1371/journal.pone.0115089
27. Malda J, Benders KEM, Klein TJ, et al. Comparative study of depth-dependent characteristics of equine and human osteochondral tissue from the medial and lateral femoral condyles. *Osteoarthritis Cartilage*. 2012;20(10):1147-1151. doi:10.1016/j.joca.2012.06.005
28. Moller NCR, Mohammadi A, Plomp S, et al. Structural, compositional, and functional effects of blunt and sharp cartilage damage on the joint: a 9-month equine groove model study. *J Orthop Res*. 2021;39(December 2020):2363-2375. doi:10.1002/jor.24971
29. Mohammadi A, te Moller NCR, Ebrahimi M, et al. Site- and zone-dependent changes in proteoglycan content and biomechanical properties of bluntly and sharply grooved equine articular cartilage. *Ann Biomed Eng*. 2022;50:1787-1797. doi:10.1007/s10439-022-02991-4
30. Look DC, Locker DR. Time saving in measurement of NMR and EPR relaxation times. *Rev Sci Instrum*. 1970;41(2):250-251. doi:10.1063/1.1684482
31. van Schie JJN, Lavini C, van Vliet LJ, Vos FM. Feasibility of a fast method for B 1-inhomogeneity correction for FSPGR sequences. *Magn Reson Imaging*. 2015;33(3):312-318. doi:10.1016/j.mri.2014.10.008
32. Hayes WC, Keer LM, Herrmann G, Mockros LF. A mathematical analysis for indentation tests of articular cartilage. *J Biomech*. 1972;5(5):541-551. doi:10.1016/0021-9290(72)90010-3
33. Jurvelin JS, Kiviranta P, Rieppo J, et al. Collagen network primarily controls Poisson's ratio of bovine articular cartilage in compression. *J Orthop Res*. 2006:690-699. doi:10.1002/jor.20107
34. Ebrahimi M, Ojanen S, Mohammadi A, et al. Elastic, viscoelastic and fibril-reinforced poroelastic material properties of healthy and osteoarthritic human tibial cartilage. *Ann Biomed Eng*. 2019;47(4):953-966. doi:10.1007/s10439-019-02213-4
35. Mäkelä JTA, Han SK, Herzog W, Korhonen RK. Very early osteoarthritis changes sensitively fluid flow properties of articular cartilage. *J Biomech*. 2015;48(12):3369-3376. doi:10.1016/j.jbiomech.2015.06.010
36. Jackson JI, Meyer CH, Nishimura DG, Macovski A. *Selection of a Convolution Function for Fourier Inversion Using Gridding*. Vol 10, 3. IEEE; 1991.
37. Kajabi AW, Casula V, Ojanen S, et al. Multiparametric MR imaging reveals early cartilage degeneration at 2 and 8 weeks after ACL transection in a rabbit model. *J Orthop Res*. 2020;38(9):1974-1986. doi:10.1002/jor.24644
38. Buckwalter JA, Lane NE. Athletics and osteoarthritis. *Am J Sports Med*. 1997;25(6):873-881.
39. Korhonen RK, Wong M, Arokoski J, Lindgren R, Helminen HJ. Importance of the superficial tissue layer for the indentation stiffness of articular cartilage. *Comparative Study*. 2002;24:99-108.
40. Xia Y. Relaxation anisotropy in cartilage by NMR microscopy (μMRI) at 14-μm resolution. *Magn Reson Med*. 1998;39(6):941-949. doi:10.1002/mrm.1910390612
41. van den Boom R, van de Lest CH, Bull SL, Brama RA, van Weeren PR, Barneveld A. Influence of repeated arthrocentesis and exercise on synovial fluid concentrations of nitric oxide, prostaglandin E 2 and glycosaminoglycans in healthy equine joints. *Equine Vet J*. 2005;37:250-256.

How to cite this article: Pala S, Hänninen NE, Mohammadi A, et al. 3D T_1 relaxation time measurements in an equine model of subtle post-traumatic osteoarthritis using MB-SWIFT. *J Orthop Res*. 2023;41:2657-2666. doi:10.1002/jor.25629